

RE J2248-511 - Not all variable, ultrasoft, X-ray AGN have narrow Balmer lines

A. A. Breeveld,¹ E. M. Puchnarewicz¹ and C. Otani²

¹ Mullard Space Science Laboratory, University College London, Holmbury St. Mary, Dorking, Surrey, RH5 6NT
² The Institute of Physical and Chemical Research (RIKEN), 2-1 Hirosawa, Wako, Saitama 351-01, Japan

ABSTRACT

We present *ASCA* data on RE J2248-511, extending existing optical and soft X-ray coverage to 10 keV, and monitoring the soft component. These data show that, despite a very strong ultrasoft X-ray excess below 0.3 keV and a soft 0.3–2 keV spectral index in earlier *ROSAT* data, the hard X-ray spectrum ($\alpha \sim -0.8$; 0.6–10 keV) is typical of type 1 AGN, and the soft component has since disappeared. Optical data taken at two different epochs show that the big blue bump is also highly variable. The strength of the ultrasoft X-ray component and the extreme variability in RE J2248-511 are reminiscent of the behaviour observed in many narrow line Seyfert 1s (NLS1s). However, the high energy end of the *ROSAT* spectrum, the *ASCA* spectrum and the Balmer line full widths at half maximum of $\sim 3000 \text{ km s}^{-1}$ in RE J2248-511 are typical of normal Seyfert 1 AGN.

The change in the soft X-ray spectrum as observed in the *ROSAT* and *ASCA* data is consistent with the behaviour of Galactic Black Hole Candidates (GBHCs) as they move from a high to a low state, i.e. a fall in the ultrasoft component and a hardening of the X-ray continuum. This GBHC analogy has also been proposed for NLS1s. Alternatively, the variability may be caused by opacity changes in a hot, optically-thin corona which surrounds a cold, dense accretion disc; this was first suggested by Guainazzi et al. for 1H0419-577, an object which shows remarkably similar properties to RE J2248-511.

Key words: Galaxies: Seyfert – Galaxies: active – Galaxies: individual: RE J2248-511

1 INTRODUCTION

The soft-to-medium X-ray spectrum (~ 0.1 –10 keV) of active galactic nuclei (AGN) is dominated by two continuum components, the soft X-ray excess (e.g. Arnaud et al. 1985; Turner & Pounds 1989; Walter & Fink 1993) and a hard X-ray power law (e.g. Turner & Pounds 1989; Comastri et al. 1992; Nandra et al. 1997). The soft excess dominates below ~ 0.5 keV and is believed to be the high energy tail of one ‘big bump’ component, of which the optical/UV big blue bump (BBB) is the low energy end (Walter & Fink 1993). A relationship between the X-ray spectrum of AGN and the velocity of the broad line regions (BLRs) has now been well established. In quasars there is an anticorrelation between the width of the $H\beta$ line and the slope of the soft X-ray spectrum in the *ROSAT* band, in the sense that the narrowest lines are seen where the slopes are softest (Laor et al. 1997, hereafter L97; Puchnarewicz et al. 1992). Boller, Brandt & Fink (1996) also demonstrated that nature usually discriminates against high velocity BLRs in ultrasoft AGN in the general AGN population. There is further evidence that the Balmer lines also ‘respond’ to the slope of the hard (*ASCA* ~ 2 –10 keV) spectrum, again with the narrow-line AGN having softer hard X-ray continua (Brandt, Mathur & Elvis 1997).

The reason for the dependence of BLR velocity on the

X-ray spectrum is not known. It has been suggested that orientation effects or black hole mass may be important (e.g. Puchnarewicz et al. 1992; L97; Grupe et al. 1998, hereafter G98; Nandra et al. 1997), although direct effects, e.g. changes in the shape of ionizing continuum affecting the structure of the BLR, may also be the cause (Rees, Netzer & Ferland 1989, Brandt et al. 1994, Puchnarewicz et al. 1997). Possible effects caused by the relative strength of the big bump component, which carries most of the ionizing continuum flux, are also poorly understood. L97 found that the 2 keV flux is relatively weak compared to the optical when the soft component is strong, which may be an important factor.

In this paper, we investigate the relative strength of the big bump and the relationship between the X-ray spectrum and BLR velocity using optical and X-ray data, including recently obtained *ASCA* data, for the Seyfert 1 galaxy RE J2248-511 ($z = 0.101$). This is a rare EUV-selected AGN which was first detected in the *ROSAT* Wide Field Camera (WFC) All Sky Survey (Pounds et al. 1993). In the associated identification programme it was shown to have broad permitted lines [$H\beta$ FWHM 2900 km s^{-1} ; equivalent width (EW) 50 \AA] (Mason et al. 1995; hereafter M95) and a very blue optical spectrum ($\alpha_{\text{opt}} \sim 0.8$; α is defined throughout as in $f_\nu \propto \nu^\alpha$, note there is no implicit negative). In a later pointed PSPC observation the 0.1–2 keV spectrum

arXiv:astro-ph/0103447v1 27 Mar 2001

overall was soft and steepened significantly at low energies ($E \lesssim 0.3$ keV) to $\alpha = -3$ (Puchnarewicz et al. 1995a; hereafter P95). Between 0.3 and 2.0 keV, the spectrum was best fitted by $\alpha = -1.6$, which is consistent with the slope of a single power law fitted to the PSPC (0.1–2 keV) spectra of other UV-bright samples (e.g. Walter & Fink 1993; Schartel et al. 1996). The very strong ultrasoft (i.e. $E < 0.3$ keV) component in RE J2248-511 has shown signs of significant variability (P95).

Thus RE J2248-511 has exhibited an unusual two-component soft X-ray spectrum. There is a significant steepening below 0.3 keV (hereafter referred to as the ‘ultrasoft’ component) and a comparatively normal spectral slope in the higher energy part of the PSPC band (hereafter the ‘soft X-ray’ component). It may well be that the soft X-ray component in RE J2248-511 is the same as the single component observed by L97 in comparable AGN, with an independent ultrasoft component superposed on top. To our knowledge, a strong ultrasoft component in addition to a normal soft X-ray spectrum, has been seen in only two other type 1 AGN (1H0419-577, Guainazzi et al. 1998; and RXJ0437.4-4711, Wang et al. 1997).

2 ASCA OBSERVATION, DATA ANALYSIS AND RESULTS

RE J2248-511 was observed with *ASCA* (Tanaka, Inoue & Holt 1994) on 1997 May 17 using the two Solid-state Imaging Spectrometer CCD detectors (SIS0 and SIS1) and the two Gas Imaging Spectrometer scintillation proportional counters (GIS2 and GIS3). The SIS detectors were operated in 1 CCD mode, using the best calibrated chips (chip 1 for SIS0 and 3 for SIS1). Faint mode was used for the entire observation, the data being converted to Bright2 mode before reduction and analysis (this allows corrections for echo effect and dark frame error). The GIS were operated in pulse height mode, and standard telemetry bit assignments were used. No lower level discriminator was used.

The data were initially processed by the Goddard Space Flight Center Guest Observer Facility using the Revision 2 screening criteria, resulting in 15.5 ks per SIS and 13 ks per GIS of acceptable data. We have used *FTOOLS*, *XSELECT* and *XSPEC* for the analysis and fitting, and have followed the recommendations of the *ASCA* Data Reduction Guide Version 2.0.

2.1 Position

RE J2248-511 is clearly detected in all four detectors. The position of the centroid of the source in the SIS detectors is RA(2000) = $22^{\text{h}} 48^{\text{m}} 40^{\text{s}}.7$, Dec.(2000) = $-51^{\circ} 09' 56''$ and in the GIS detectors is RA(2000) = $22^{\text{h}} 48^{\text{m}} 38^{\text{s}}$, Dec.(2000) = $-51^{\circ} 09' 20''$. These measurements compare well with the previous optical measurement of RA(2000) = $22^{\text{h}} 48^{\text{m}} 41^{\text{s}}.2$, Dec.(2000) = $-51^{\circ} 09' 54''$ (M95), given that the error on the GIS position is at least 50 arcsec. There is no evidence that the source is extended and there are no other significant X-ray sources in the field of view.

2.2 Spectral analysis

We used circular extraction regions, centred on the object, with radii of 4, 3, 6 and 6 arcmin for SIS0, SIS1, GIS2 and

GIS3 respectively. A radius of 4 arcmin is recommended for the SIS, but in the SIS1 the object lies too close to the edge of the CCD to use a full 4 arcmin radius. Using a square region, or a larger, but offset, circular region, instead of the 3 arcmin circle chosen, does not affect the result significantly. We have carefully chosen circular, source-free extraction regions for the background. For the SIS the background is taken from the same chip as the source, whereas for the GIS, the background is taken from a region at the same radius as the source from the optical axis of the telescope.

We have extracted spectra from inside the specified extraction regions using all of the acceptable exposure times. The SIS spectra were grouped to give 20 counts in each bin, and the GIS spectra 40 counts per bin. Suitable response files were generated for each detector. Only events with grades 0,2,3,4 were selected from the SIS data.

Using *XSPEC*, we first fitted the spectra from the two SIS detectors simultaneously, and then from the two GIS detectors. The fits are given in Table 1. The two sets of results were consistent within 1σ , with the GIS giving slightly harder slopes than the SIS. The data from all four detectors were therefore simultaneously fitted to the same model, with the relative normalizations allowed to go free, to allow for small calibration uncertainties in the absolute normalization in each detector. We fixed the local Galactic column at $N_{\text{HGal}} = 1.4 \times 10^{20} \text{ cm}^{-2}$ (interpolated from the maps of Stark et al. 1984, see P95), and left the column of the host galaxy (the intrinsic column N_{HInt}), at redshift 0.1, to be a free parameter, but greater than or equal to zero. A single, absorbed power law gave a good fit ($\chi^2_{\nu} = 0.89$) over the range 0.5–10.0 keV (SIS) 0.7–10.0 keV (GIS), with $\alpha = -0.85^{+0.08}_{-0.05}$ and $N_{\text{HInt}} = 1.76 \pm 4.4 \times 10^{20} \text{ cm}^{-2}$. The data and fit are shown in Fig. 1. The errors $\Delta\alpha$ and ΔN_{HInt} in the fit were calculated by making a grid search for models with $\Delta\chi^2 = 4.61$, as appropriate for a 90 per cent confidence level for two interesting parameters (e.g. Press et al. 1989). Ignoring data below 1.0 keV leads to a slightly harder $\alpha = -0.83 \pm 0.08$ although it is obviously very close to the 0.5–10 keV fits.

An additional error comes from N_{HGal} itself. P95 use a 10 per cent uncertainty, as calculated by Laor et al. 1994. Stark et al. (1992) suggest an error 3 times larger than this, making our value for $N_{\text{HGal}} = 1.4 \times 10^{20} \pm 6 \times 10^{19} \text{ cm}^{-2}$. For safety, and because the declination is below -40° , we have assumed the larger error and explored the effect on the fits given in Table 1. We also found the 90 per cent confidence limits on the fit after propagating through the maximum and minimum values for N_{HGal} . These limits have been included in the table as a second set of errors where they are outside the previous confidence limits. In the fitting to these *ASCA* data, the change in N_{HGal} has very little effect on α .

In order to increase the spectral resolution at low energies to check for any interesting features (e.g. warm absorber edges), we combined the data from SIS0 and SIS1 in the manner described in the *ASCA* guide to make a single SIS spectrum. The background files and exposures were calculated carefully and the final PHA file was grouped to 20 counts per bin. Again a single, absorbed power law gave a good fit ($\chi^2_{\nu} = 0.48$) with $\alpha = -0.83 \pm 0.1$ and $N_{\text{HInt}} = 0^{+4.6}_{-9.1} \times 10^{20} \text{ cm}^{-2}$, which is not significantly different from the fit to all four detectors simultaneously, as expected. No additional features were required to fit the data. The re-

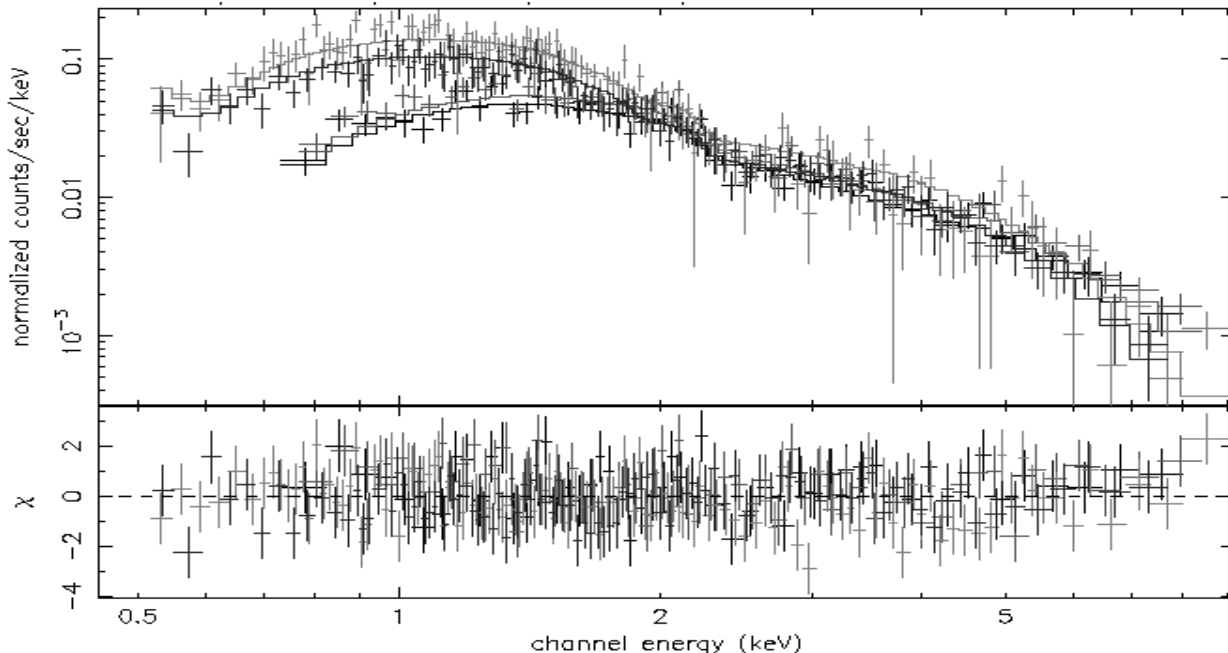


Figure 1. The best fitting single power law fitted simultaneously to the SIS and GIS data. The residuals to the fit, in the lower window, are in units of $\Delta\chi^2$

duced chi-squared values are very low, implying that the error bars may be larger than necessary in the combined data. This is probably associated with the method of combining the response matrices. Never-the-less, in all the power-law fits so far described, the slopes are consistent within their errors which suggests that the result is robust (see Table 1). For convenience, the combined spectrum has been used later on for comparison with the *ROSAT* data.

George et al. (1998) comment that there are uncertainties in the XRT/SIS effective area at energies below 0.6 keV and especially around 0.5 keV. For this reason we have also included fits ignoring data below 0.6 keV to check the consistency of the data (see Table 1). The *ASCA* Guest Observer Facility quantify this uncertainty and give a guideline of $2 \times 10^{20} \text{ cm}^{-2}$ as a 90 percent systematic error on the SIS for measurement of the line of sight column density (see also Dotani et al. 1996). This factor has been taken into account in the comparison between *ASCA* and PSPC data (see Table 2 and Section 2.3.1).

We tried two component fits to the data to see if there were any break in the power-law slope, or an excess at low energies. A broken power law or two power laws gave no improvement in χ^2 . Adding a black body at 220 eV gave a small improvement in χ^2 , but according to the F-test (see e.g. Bevington 1969), the improvement is not significant.

2.2.1 FeK α line

In almost all Seyfert 1 AGN observed with *ASCA* an FeK α fluorescent line is significantly detected at 6.4 keV (neutral) or 6.7 keV (ionized), with an average EW of 121 ± 16 eV (Nandra et al. 1997). The EW tends to be smaller for higher luminosity objects and these lines are rarely seen in quasars.

To test for FeK α emission in RE J2248-511, we added

an unresolved Gaussian emission line to the power-law fit to the *ASCA* simultaneous SIS and GIS data. According to the F-test, the additional component did not provide a significant improvement at either 6.4 or 6.7 keV. Allowing the width of the Gaussian line to vary as a free parameter gave an unrealistically large FWHM and EW (13 keV FWHM and 6 keV EW) while making the underlying power-law continuum very steep. The upper limits (90 per cent) on the EW of a narrow line added at 6.4 or 6.7 keV are 220 eV and 335 eV, respectively. These are above the average given by Nandra et al. (1997), although a lack of significant FeK α emission would not be unexpected since the luminosity of RE J2248-511 ($L \sim 10^{45} \text{ erg s}^{-1}$; $H_0=50 \text{ km s}^{-1} \text{ Mpc}^{-1}$, $q_0=0$) places it on the borderline between a Seyfert 1 and quasar.

2.2.2 Short term variability

During the pointed *ROSAT* observation, the flux of RE J2248-511 fell by 14 per cent in 16 hours (P95). The mean *ASCA* count rates for SIS0, SIS1, GIS2 and GIS3 respectively were 0.209 ± 0.006 , 0.156 ± 0.004 , 0.106 ± 0.003 , $0.123 \pm 0.003 \text{ count s}^{-1}$. Light curves were prepared from these *ASCA* data with bin sizes of 204, 264, 388 and 335 s respectively, to give a minimum of 50 counts per bin. The deviation from constant was given by $\chi^2/\text{dof} = 164/107$, $98/79$, $34/53$ and $73/63$ for SIS0, SIS1, GIS2 and GIS3 respectively. Thus, there is no significant variability observed in the light curves of any of the detectors, over a period of ~ 17 hours.

Table 1. Power-law fits to ASCA GIS and SIS data

	Range (keV)	N_{HGal}^a	α	Norm ^b	χ^2/dof	χ^2_ν
SIS0+SIS1	0.5–10.0	$2.1^{+4.6}_{-4.2} +5.3_{-4.8}$	$-0.9^{+0.1}_{-0.09}$	1.4 ± 0.1	170/228	0.74
GIS2+GIS3	0.7–10.0	0^{+0}_{-25}	-0.87 ± 0.09	1.5 ± 0.1	111/113	0.98
SIS+GIS	0.5(SIS)/0.7(GIS)–10.0	$1.76^{+3.7}_{-3.5} +4.4_{-4.1}$	$-0.85^{+0.08}_{-0.05}$	1.4 ± 0.1	307/346	0.89
SIS+GIS	1.0–10.0	0^{+0}_{-22}	-0.83 ± 0.08	1.3 ± 0.1	246/288	0.85
SIS combined	0.5–10.0	$0^{+3.5}_{-4} +4.1_{-4.8}$	-0.83 ± 0.12	1.5 ± 0.05	86/178	0.48
SIS combined	0.6–10.0	$0^{+4.3}_{-8.6} +4.6_{-9.1}$	-0.83 ± 0.1	1.5 ± 0.05	82/171	0.48
SIS combined	1.0–10.0	0^{+0}_{-40}	-0.83 ± 0.12	1.5 ± 0.1	65/144	0.45

A value of $1.4 \times 10^{20} \pm 6 \times 10^{19} \text{ cm}^{-2}$ has been assumed for the Galactic column density.

The errors were calculated by making a grid search at the 90 per cent confidence level (i.e. with $\Delta\chi^2 = 4.61$), for two interesting parameters. The second set of errors, where given, are calculated assuming the maximum and minimum values for N_{HGal} .

^a $\times 10^{20} \text{ cm}^{-2}$. The value is constrained to be greater than zero although the errors have been allowed to go below zero.

^b $\times 10^{-3} \text{ photons cm}^{-2} \text{ s}^{-1}$ at 1 keV

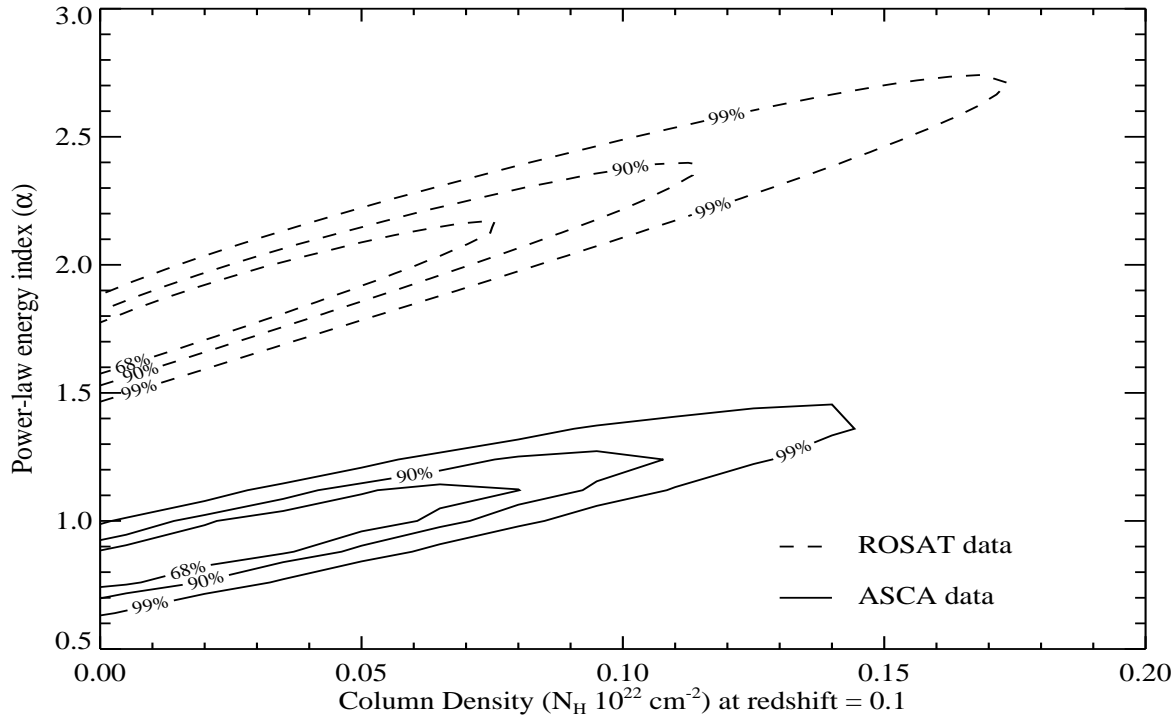


Figure 2. Confidence contours at the 68, 90 and 99 per cent level for the *ROSAT* PSPC and *ASCA* SIS data fitted independently to single power-law models, over energy range 0.5–2 keV, showing that the two data sets are different at more than 99 per cent significance. Note however that the column density is consistent for both data sets while the power-law index is different.

2.3 Long term variability

2.3.1 Comparison between *ROSAT* PSPC, *WFC* and *ASCA* data

The pointed *ROSAT* PSPC data taken in 1993 were shown by P95 to have a higher soft X-ray excess than that expected from the original *WFC* observation, suggesting a variable soft X-ray component. To test for further evidence of long term variability in the soft X-ray component, we re-reduced the *ROSAT* PSPC data using the same method as P95, and we find results that agree with the best fitting model given in that paper (see Section 1). P95 examined the possibility

that there could be a ‘hole’ in the galactic hydrogen column (N_{HGal}), such that the measured value was greater than the true value, making the ultrasoft component appear stronger than it really was. However, P95 were able to reject this hypothesis by comparison of several N_{HGal} measurements and also *IRAS* data.

The power law which had given a good fit to the *ASCA* SIS combined data failed to reproduce the PSPC data at greater than 99 per cent confidence. Simultaneous fits to the SIS combined data and the PSPC were unsatisfactory: both a broken power law and a black body combined with a power law converged to $\chi^2_\nu = 2.8$.

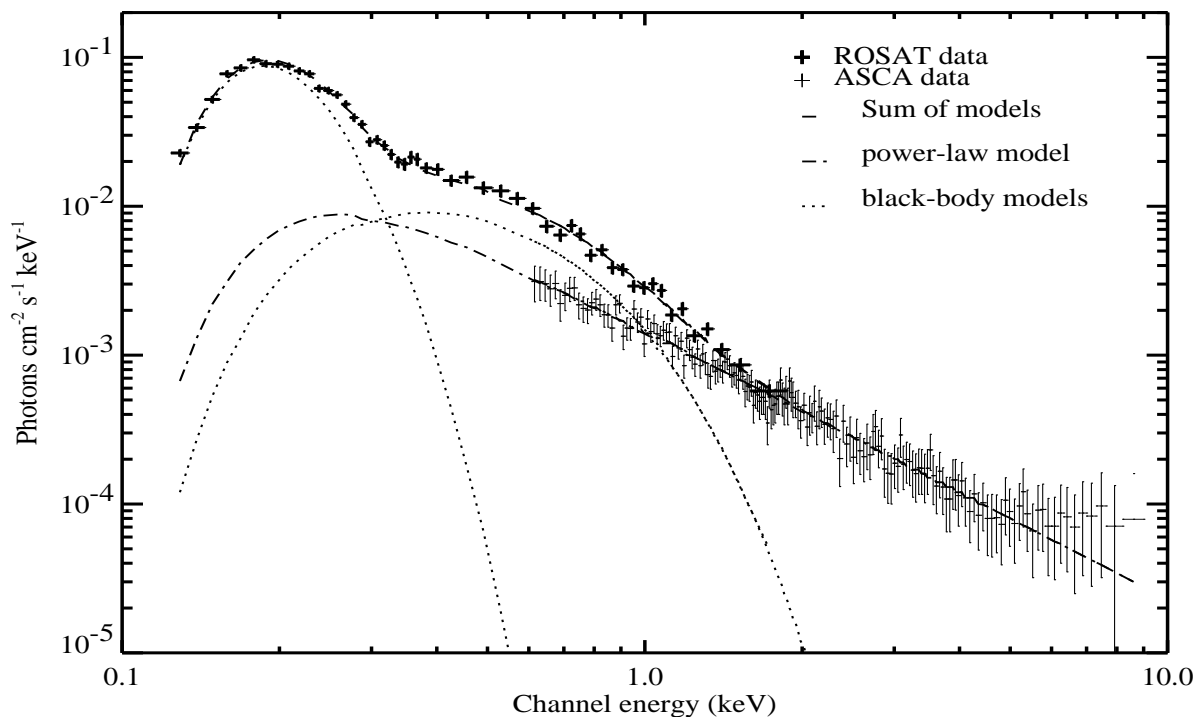


Figure 3. The *ASCA* data is fitted to a single power-law model while the *ROSAT* PSPC data is fitted to a composite model consisting of the *ASCA* power law, plus two black bodies.

To assess the extent to which the spectrum had changed, the PSPC and *ASCA* data were compared only in the overlapping energy range, 0.5–2.0 keV. The PSPC and SIS spectra were each fitted with an absorbed power law, with the local N_{Hint} allowed to go free, and the two sets of confidence contours are plotted in Fig. 2. This shows that the 0.5–2.0 keV spectra are different at more than 99 per cent significance, although the Hydrogen column is consistent with being the same for both data sets. These data were then fitted simultaneously, constraining N_{Hint} to be the same for both data sets while freezing N_{HGal} at $1.4 \times 10^{20} \text{ cm}^{-2}$, but allowing different power-law slopes and normalizations. The resulting intrinsic Hydrogen column was $1.5 \times 10^{20} \text{ cm}^{-2}$ and the PSC spectrum was soft with $\alpha = -1.8$, whereas the SIS data were hard with $\alpha = -0.9$. Table 2 gives the results from the fitting of SIS and PSPC data separately and simultaneously. Thus it appears that the 0.5–2 keV spectrum was significantly harder when the *ASCA* data were taken.

In fitting the 0.5–2 keV PSPC data, it should be noted that even this restricted band has some contamination from lower energy emission due to the limited energy resolution of the PSPC ($\Delta E/E = 0.4/\sqrt{E/\text{keV}}$; Walter & Fink 1993). In order to test whether the contamination could disguise consistency between the PSPC and *ASCA* data, we simulated the PSPC data as a broken power law, assuming a slope consistent with *ASCA* (-0.9) above 0.5 keV. The amount of ‘contamination’ was gradually increased by adjusting the slope of the lower energy power law until a single power law (0.5–2.0 keV) fitted to this simulation gave a slope of -1.4 , which would be just consistent with the real PSPC fit at the 1 percent confidence level (see Figure 2). The sim-

ulated lower energy power law required a slope steeper than -6.0 to reproduce the real fitted parameters, and this is much steeper than is observed.

Spectral indices as measured by the PSPC are believed to be systematically steeper than those measured by other instruments in overlapping wavelength ranges. The difference has been estimated to be between 0.2 (Fiore et al. 1994) and 0.4 (Iwasawa, Brandt & Fabian 1998, Iwasawa, Fabian & Nandra 1999), depending on the shape of the spectrum being measured. The possible systematic error of $2 \times 10^{20} \text{ cm}^{-2}$ on the SIS measurement of N_{Hint} described in Section 2.2 may also affect the comparison. As an apparent column density less than this value is probably not significant, the SIS fit in Table 2 was repeated with N_{Hint} forced to be zero. This resulted in a slightly harder power-law slope of -0.88 and no significant change to the other values. The power-law fit in Table 2 was also repeated with N_{Hint} $2 \times 10^{20} \text{ cm}^{-2}$ less for the SIS data than the PSPC data. This led to the two slopes getting slightly closer together with α changing from -1.8 to -1.7 for the PSPC and from -0.9 to -0.95 for the SIS. By examining the contour plot in Fig 2, it can be seen that with this change in the slope of the SIS data, and a reduction in the PSPC slope of 0.5, there is only just an overlap at the 99 percent level. Thus, even including the most pessimistic systematic errors on both the PSPC and SIS data, it is very unlikely that the PSPC and SIS measurement can be consistent with one another.

It may be that the change in the spectral slope between the PSPC and *ASCA* spectra is due to variability in a soft component only, while the hard component stayed constant throughout. To test this, we re-fitted the PSPC

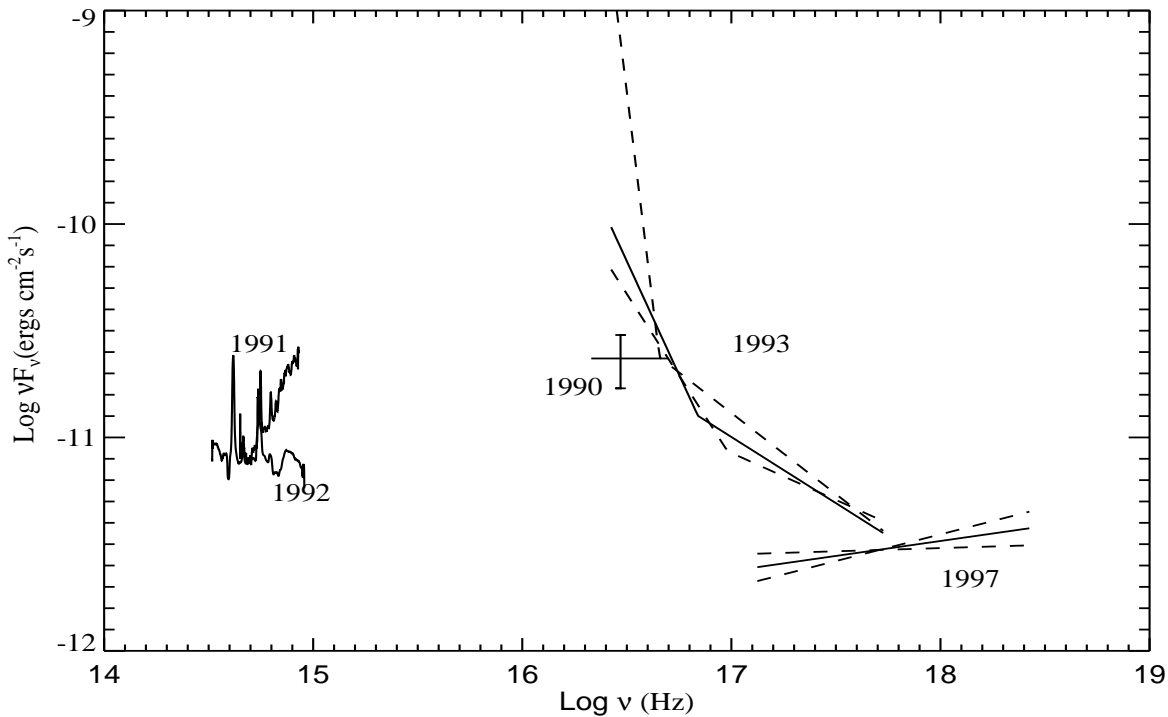


Figure 4. This multiwavelength spectrum includes: the WFC RASS observation and the pointed PSPC data (P95) plotted as a broken power law; the *ASCA* data described here plotted as a single power law; the optical data (M95); and the optical data taken by G98.

data assuming that a power-law component, consistent with that measured from the *ASCA* data, extended through the ROSAT range. Various soft components were added to complete the model fit to the PSPC data. The power law (slope, flux and intrinsic column density) for the hard component was fixed from fitting to the SIS data (for the 0.5–10 keV range; $N_{\text{Hint}} = 0 \text{ cm}^{-2}$ and $\alpha = -0.83$; see Table 1) and the additional soft components tried included blackbodies, Bremsstrahlung components and additional power laws. The best fitting model ($\chi^2_\nu = 1.2$) was obtained by adding a combination of two black bodies, one at $kT_{\text{bb}} = 28 \text{ eV}$ and the other at $kT_{\text{bb}} = 160 \text{ eV}$ (see Table 2).

Fig. 3 shows both the SIS and the PSPC spectra together with the underlying power law, which fits the SIS data on its own, and the two additional black body components which are required to fit the PSPC data. This illustrates the nature of the variability of the soft X-ray spectrum. The *ASCA* data cannot be used to constrain the presence of the lower temperature (28 eV) black body, but an upper limit on the flux of the higher temperature (160 eV) black body is 10 times less than the ROSAT fit, at 99 per cent certainty. The flux in the higher temperature black body is $4.3 \times 10^{-12} \text{ ergs cm}^{-2} \text{ s}^{-1}$ (luminosity $2 \times 10^{44} \text{ ergs s}^{-1}$), thus a change in flux of at least $3.9 \times 10^{-12} \text{ ergs cm}^{-2} \text{ s}^{-1}$ has been observed. If the whole of the lower temperature black body has also disappeared, this gives an upper limit on the flux change of $7.2 \times 10^{-12} \text{ ergs cm}^{-2} \text{ s}^{-1}$. For comparison, the flux in the power law (2–10 keV) is $4.6 \times 10^{-12} \text{ ergs cm}^{-2} \text{ s}^{-1}$ (luminosity $2.2 \times 10^{44} \text{ ergs s}^{-1}$).

The original WFC RASS observation with a count rate of $18 \pm 5 \text{ count ks}^{-1}$ in detector S1a (covering the band

90–206 eV; Wells et al. 1990) was found by P95 to be inconsistent with the later PSPC observation, from which the best fitting power-law model predicted a WFC count rate of $38 \pm 6 \text{ count ks}^{-1}$. The RASS PSPC data have been described by G98 as having a slope of $\alpha = -1.9 \pm 0.1$ with a negative N_{H} ($N_{\text{Hint}} \sim -0.5 \times 10^{20} \text{ cm}^{-2}$). If this were modelled with the Galactic N_{H} , it would require a softening at the lowest energies. Using the model of G98 we predict a count rate of $29 \pm 4 \text{ count ks}^{-1}$ in S1a of the WFC, which is higher than that measured, but not by more than 2σ significance, which is allowable given the calibration uncertainties at the lowest energies in the PSPC. No direct comparison can be made between the WFC data and the *ASCA* data because there is no overlap between the detectors. Extrapolating the *ASCA* spectrum to the WFC range however gives a prediction of less than 1 count ks^{-1} .

2.3.2 Variation in optical data

G98 describe optical spectroscopy of RE J2248-511 taken in 1992. These data were taken in photometric conditions with a 2 arcsec slit. Whilst they were not taken at the parallactic angle, the zenith distance of the object was high when the spectrum was taken and a comparison with CCD images shows that no blue light has been lost through refraction (H.-C. Thomas, private communication, 1998). G98 measure a slope in the optical of $\alpha = -1.3$, much softer (i.e. redder) than the $\alpha = +0.8$ measured from the 1991 M95 data. We have plotted their optical data in Fig. 4 for direct comparison with the M95 data. Assuming a conservative systematic error of 30 per cent on the M95 spectrum,

Table 2. Spectral fits to ASCA SIS and ROSAT PSPC data

Model	Range (keV)	N_{Hint}^a	α	Norm ^b	kT_{bb} (eV)	Norm _{bb} ^b	χ^2 /dof	χ^2_ν
PSPC	0.5–2.0	$1.15^{+10.4}_{-4.0}$	$-1.8^{+0.4}_{-0.6}$	2.9 ± 0.3			25.2/19	1.3
SIS	0.5–2.0	$2.2^{+8.3}_{-5.4}$	-0.98 ± 0.34	1.6 ± 0.07			58/96	0.60
power law ^c	0.5–2.0	$1.5^{+6.4}_{-4}$	-1.8 ± 0.15 (P) -0.9 ± 0.13 (S)	2.9 ± 0.1 (P) 1.5 ± 0.5 (S)			83.5/116	0.71
PSPC PL + 2bb ^d	0.1-2.0	0	-0.83	1.5	28 ± 1.2 160 ± 6	0.76 ± 1.8 0.06 ± 0.08	57.85/48	1.2

A value of $1.4 \times 10^{20} \text{ cm}^{-2}$ has been assumed for the Galactic column density.

(P) and (S) indicate values associated with the PSPC or SIS only, respectively.

‘bb’ is used to indicate black body.

^a $\times 10^{20} \text{ cm}^{-2}$

^b $\times 10^{-3} \text{ photons cm}^{-2} \text{ s}^{-1}$ at 1 keV

^c fitting the SIS and PSPC data simultaneously, but allowing the spectral slope and normalization to vary independently.

^d PSPC data fitted to a fixed power law and normalization determined from the SIS (see Table 1) plus an additional two black bodies.

we find that the fluxes in the two optical spectra are not inconsistent, although the continuum slope has changed dramatically. In the two spectra, the continuum fluxes are approximately equal at the wavelength of $H\beta$, and the emission line FWHM, EW and fluxes of the $H\beta$ lines are very similar. Whilst the FWHM and fluxes of the $H\alpha$ lines are also similar, the $H\alpha$ EW is higher in the M95 data, and is associated with a lower continuum level at this wavelength. However, given the possible errors on the absolute flux measurements, we cannot say for certain whether the line fluxes have stayed constant.

2.3.3 Multiwavelength spectrum

Fig. 4 shows the multiwavelength spectrum including the pointed PSPC and ASCA data together with the optical data. The WFC point is also included. Significant changes in the overall optical to X-ray spectrum are obvious. In X-rays, one interpretation could be that the soft component was strong in 1990, steepened further at the lowest energies in 1993 but then fell away completely in 1997 (note, though, the caveats in Section 2.3.1). Meanwhile, the BBB was unusually strong during 1991, yet by 1992 there was little or no emission from this component. These data suggest many intriguing possibilities for the behaviour of the optical to X-ray spectrum in RE J2248-511. For example, if the BBB and the ultrasoft component are part of one ‘big bump’, the flux in this component may be changing dramatically from very low levels to where it dominates the spectrum completely. Alternatively, the big bump may be shifting in frequency, i.e. changing its characteristic temperature significantly. It is also possible that the BBB and ultrasoft component are independent features and there is no commonality in their behaviour.

3 DISCUSSION

Optical and X-ray spectra of RE J2248-511 have now been measured over a period of seven years and reveal extreme

changes in both ranges. In this paper, we present the results from a new ASCA measurement and compare it with previous ROSAT (PSPC and WFC) and optical data.

The pointed RE J2248-511 PSPC data, modelled with a single power-law in the full 0.1–2 keV range (for fixed Galactic N_{H}) gives a very poor fit (P95). It is necessary to use a broken power law with a soft index (below 0.26 keV) of -3.13 and a hard index -1.62 . The ASCA X-ray spectrum (0.5–10 keV), on the other hand, is well fitted by an $\alpha = -0.85 \pm 0.08$ power law with no evidence for any curvature, soft excess, or excess absorption. This is consistent with the mean ASCA energy index determined for broad line Seyfert 1s by Brandt et al. (1997) who measured -0.87 ± 0.036 . Similarly, Comastri et al. (1992) found a mean 2–10 keV slope of -0.89 ± 0.06 , with most objects distributed around $\alpha \sim -1.0$, from an EXOSAT sample of AGN. Thus despite the unusual two-component low energy X-ray spectrum measured by the PSPC in 1993, RE J2248-511 had a high energy X-ray continuum typical of AGN in general at the time of the ASCA observation, with no sign of any soft X-ray excess.

In Section 2.3.1, we showed that the changes between the PSPC and the ASCA spectrum observed were consistent with a changing soft X-ray spectrum (modelled by two blackbodies, $kT_{\text{eff}} = 28 \text{ eV}$ and 160 eV) superposed on an invariant, underlying $\alpha = -0.8$ power law. However, while the lack of any ‘soft X-ray’ component emission in the ASCA spectrum is ably demonstrated by these data, the slope of any underlying power-law in the earlier PSPC spectrum is very poorly constrained. The ‘ultrasoft’ component in the PSPC spectrum (modelled by the 28 eV black body) is below the spectral range covered by ASCA and therefore cannot be compared with the later spectrum. Note, however, that we have no evidence that the ‘ultrasoft’ and ‘soft’ X-ray components are in fact separate components; produced by different mechanisms and varying independently. We can only say that the shape of the spectrum does not conform to a single power law or single blackbody.

3.1 RE J2248-511 compared with PG quasars

With an absolute magnitude $M_B < -23$, RE J2248-511 meets the definition of a quasar given by Schmidt & Green (1983) for the PG Bright Quasar survey. At $z = 0.101$, and with a Galactic column density $N_{\text{HGal}} = 1.4 \times 10^{20} \text{ cm}^{-2}$, it is directly comparable with the L97 sample of PG quasars*. L97 found no evidence for spectral curvature in their sample and the L97 mean spectral index in the *ROSAT* PSPC energy range (0.1–2 keV) is $\alpha \sim -1.7 \pm 0.1$.

If we consider only the slope of the RE J2248-511 ‘soft X-ray’ component above 0.3 keV, in both the pointed and the RASS RE J2248-511 PSPC observations, it appears typical of the L97 sample. Similarly, given the slope of the 0.3–2 keV spectrum, the optical to X-ray ratio of RE J2248-511 is consistent with their sample with $\alpha_{\text{ox}} = -1.3$ (using the definition of α_{ox} of L97 i.e. the slope between 3000Å and 2 keV). In other words, RE J2248-511 exhibits an otherwise flat, normal, underlying optical to X-ray continuum; what sets this object apart is the apparent superposition of an unusually strong ultrasoft (<0.3 keV) component.

Most of the optical slopes from L97 (α_{opt}) are small and negative (with a mean of -0.36 ± 0.22). None are as hard (blue) as the 1991 measurement of RE J2248-511, when an $\alpha_{\text{opt}} \sim 0.8$ was observed. In 1992 however, the index of the optical continuum fell to -1.3 , much *softer* (redder) than the L97 quasars; another dramatic change in the shape of the continuum of RE J2248-511.

3.2 The X-ray spectrum and the BLR

Before any investigation of the relationship between the BLR and the soft X-ray component can be made, it is essential to establish the phenomenology of the AGN, i.e. whether or not it can be described as ‘ultrasoft’. In Boller et al. (1996), the average slope, quantified by a single power-law fit to the 0.1 to 2.4 keV *ROSAT* PSPC band, was used to assess the softness of the Seyfert galaxies. However, it does not take into account any significant curvature in the spectrum, so that AGN like RE J2248-511, whose PSPC spectrum rises steeply below 0.3 keV (P95), may have been overlooked. For example, when the PSPC spectrum of RE J2248-511 is fitted with a single power law (where the local column density is fixed to the Galactic column), the power-law index α converges to -1.8 , which is not particularly soft when compared with other AGN. Taking this index together with the Balmer line FWHM of $\sim 3000 \text{ km s}^{-1}$, the object does not lie in the zone of avoidance as described by Fig. 8 in Boller et al. (1996). However, with a χ^2_{ν} of 2.4 (for 49 degrees of freedom), a single power law is an unacceptable fit to the spectrum. A concave broken power law provided the best fit, with a low energy slope (<0.3 keV) of $\alpha = -3.2$ (a $\chi^2_{\nu} = 1$ for 49 degrees of freedom), thus model fitting indicates that RE J2248-511 does have a very steep, soft X-ray excess.

Furthermore, the original definition of an ultrasoft source was made by Puchnarewicz et al. (1992) and Córdova et al. (1992). An ultrasoft source had to satisfy the criterion that the C1 to C2 count rate ratio must exceed 2.8, where

* L97 selects bright PG quasars with low redshift ($z \leq 0.4$) and local Galactic column density ($N_{\text{HGal}} < 1.9 \times 10^{20} \text{ cm}^{-2}$)

C1 covers the 0.16 to 0.56 keV band of the *Einstein* IPC detector and C2 covers the 0.56 to 1.08 keV range. By folding the best-fitting PSPC model through the IPC response, we find that the C1 to C2 ratio for RE J2248-511 is 3.1; thus satisfying the criterion for an ultrasoft AGN.

We find, therefore, that RE J2248-511 is a variable, ultrasoft X-ray AGN with broad lines (Balmer line FWHM $\sim 3000 \text{ km s}^{-1}$). The presence of broad lines is unusual for an ultrasoft AGN (Puchnarewicz et al. 1992), consequently this source is very important in our understanding of the relationship between the BLR velocity and the soft X-ray excess.

In 2.3.2 the two optical spectra of RE J2248-511 were described. If the Balmer line fluxes and FWHM have remained the same between 1991 and 1992, the data suggest that the changes in the central ionizing continuum have not affected either the velocity of the outer BLR, nor the line strengths, at least not on a timescale of about a year.

Baldwin et al. (1995) showed that efficient line emission occurs where the combination of conditions in the gas and the nature of the ionizing continuum are optimized. Thus it is possible that clouds may cover a wide region but are only ‘lit-up’ where these conditions are right. If the FWHM of the Balmer lines in RE J2248-511 have remained unchanged throughout the very large variations in ionizing continuum strength and shape, this would suggest either that this fine-tuning takes a long time to respond (more than a year), or that there is no low-velocity gas in RE J2248-511.

3.2.1 The big bump and the soft X-ray spectrum

It has been suggested that the soft X-ray excess is the upper energy tail of the big blue bump, although studies have been unable to prove a direct relationship between these two components. However, the correlation between α_x and the Balmer line FWHM links the velocity of the outer broad line region with the shape of the soft X-ray spectrum. RE J2248-511 is consistent with this trend *if* the 0.3-2 keV part of the PSPC spectrum *only* is considered.

One major difference between RE J2248-511 and other Seyfert 1s is the presence of the ultrasoft component which is very variable. Another is the very hard (blue) optical continuum, which is also very variable. We speculate that these unusual X-ray and optical continua may be related, i.e. that they may be part of a very strong and variable big bump. The Balmer line region velocity is not affected by the presence of the ultrasoft component but *is* consistent with the slope of the soft X-ray component. However, since the α_{ox} for RE J2248-511 is typical of the L97 quasars given its α_x , some relationship between the big bump and the soft X-ray spectrum cannot be ruled out.

3.3 Comparison with other ultrasoft AGN

There are several other ultrasoft AGN which have shown dramatic variability in the soft component, such as RE J1237+264, (Brandt, Pounds & Fink 1995) and WPVS 007 (Grupe et al. 1995). These objects are both NLS1s and showed a reduction in the soft component by factors of 70 and 400 respectively. E1615+061 (Piro et al. 1988), however, is an ultrasoft, broad line object which showed variability such that it became less soft when it became less luminous.

The object 1H0419-577 (Marshall, Fruscione & Carone 1995, Fruscione 1996) shows remarkably similar characteristics to RE J2248-511 (Guainazzi et al. 1998). It is categorized as a Seyfert 1.5 with a redshift of 0.103 and has a strong, broad $H\beta$ component of FWHM 3500 km s^{-1} . The PSPC data are not well fitted by a simple power law due to a softening at low energies, and require a broken power law, or a power law plus an additional soft component (i.e. black body, Bremsstrahlung or another power law). The blackbody temperature of the ultrasoft component is around 40 eV. A comparison of *ROSAT* PSPC, *ASCA* and *Beppo-SAX* data revealed a highly variable soft component and little evidence of iron lines at around 6.4–6.7 keV.

RX J0437.4-4711 (Wang et al. 1997) is another ultrasoft Seyfert 1 ($z = 0.051$) whose PSPC data cannot be described by a single power law, but requires an ultrasoft component. This component can be described by a black body with a temperature of 22 eV. Large amplitude flux variability has been observed in the *ASCA* range. This object differs from RE J2248-511 in that it has an unusually steep *ASCA* slope for a broad line object ($H\beta \sim 4300 \text{ km s}^{-1}$) with $\alpha \sim -1.2$.

3.4 Models of the X-ray spectrum

3.4.1 Accretion discs

Comptonized accretion disc models have been used successfully to model the continuum production in AGN. For example, the hot corona model proposed by Haardt & Maraschi (1993), describes a feedback system whereby medium energy X-rays from a hot, optically-thin corona are reprocessed by a cold, dense accretion disk into soft blackbody photons. Some of these blackbody photons become seeds for Comptonization in the hot corona, forming a medium to high energy X-ray continuum (see also Haardt, Maraschi & Ghisellini 1997). Their models can simulate systems in which the X-ray power-law slope changes in response to changes in flux from the source, and changes in opacity in the corona. The spectral changes observed in both 1H0419-577 and RE J2248-511 can be explained by their model, by invoking a change in opacity (τ) from ~ 1 to ~ 0.1 . The corona cannot be electron-positron pair dominated, because this would require even a small change in spectral index to be accompanied by a change in flux larger than a factor of 2, which is not observed. Guainazzi et al. (1998) discuss the Haardt et al. (1997) model with respect to 1H0419-577, and also viscousless, two-phase shock accretion disk models by Chakrabarti & Titarchuk (1995) and Ebisawa, Titarchuk & Chakrabarti (1996). In the latter model, the changes in the 1H0419-577 spectrum are assigned to a transition from a bulk motion to a thermal motion regime due to a change in accretion rate.

Pounds, Done & Osborne (1995) have suggested that the NLS1 RE J1034+396 is a high- M analogue of a Galactic Black Hole Candidate (GBHC) in a high state. In this state, the ultrasoft component is steep and soft, while the hard component is very weak and variable but is also soft relative to the low-state slope in hard X-rays. Further evidence for this GBHC model was given by Brandt et al. (1997), who found that the *ASCA* slopes of NLS1s in general are soft relative to broad line Seyfert 1s (see also G98). With the ultrasoft component in RE J2248-511 switching from a high to

a low state, it could also be a candidate for the GBHC analogy, although one that fits uneasily into the NLS1 scenario because of its broad lines. However, the disappearance of the soft component and hardening of the X-ray power-law are consistent with the behaviour of GBHCs. Further investigation of this model would require simultaneous monitoring of the soft and hard X-ray spectra (i.e. from 0.1 to ~ 10 keV or higher) however; the present data are insufficient.

3.4.2 Reprocessing models

Collin-Souffrin et al. (1996) found that the near-IR to X-ray spectra of AGN can be modelled by a system of radiatively heated clouds, optically thick to electron scattering, with a covering factor greater than 0.5. These clouds could be in a ‘quasi-spherical’ distribution or a thick disk. The X-ray spectrum produced by this model is a combination of the primary incident continuum (assumed to be a featureless $\alpha = 1$ power law) and the component reflected from the hot, illuminated side of the clouds. (The optical/UV emission is produced by the cooler, unilluminated side of the clouds.) In order to predict an ultrasoft excess of the strength observed in RE J2248-511, the spectrum must be dominated by the reflection component. However, in this case the $\text{FeK}\alpha$ line would also be strong, yet only an upper limit could be measured from the *ASCA* data of RE J2248-511. Variability studies would provide further evidence relevant for this model since it predicts that the UV should respond on longer timescales than X-rays, although which wavelength leads will depend on the geometry of the system.

4 CONCLUSIONS

RE J2248-511 has displayed a most unusual low energy X-ray spectrum for any type 1 AGN. A steep, variable, ultrasoft component is found below 0.3 keV, which appeared from earlier *ROSAT* data to be superposed on a relatively normal soft X-ray spectrum. RE J2248-511 has also exhibited an extremely blue, but variable, optical spectrum. The broad Balmer line widths are consistent with α_x above 0.3 keV and appear to be unaffected by the strength of the big blue bump.

The *ASCA* spectrum presented in this paper has shown the soft X-ray component (0.5–2 keV) also to be highly variable, falling away to the extent that it is no longer detectable. The hard X-ray (0.5–10 keV) continuum can be fitted with a single, absorbed power law of slope $\alpha \sim -0.85$ which shows no indication of short timescale variability. Neither does it show significant evidence for absorption edges or emission lines. It may be extrapolated through the *ROSAT* PSPC spectrum taken 4 years earlier, if the soft excess measured then is modelled by two blackbodies ($kT_{\text{eff}} = 28$ eV and 160 eV).

The spectral changes are similar to those observed in GBHCs as those systems fall into a low from a high state. In the high state, the ultrasoft component is strong and the hard X-ray continuum is soft, while in the low state the ultrasoft component falls away and the hard power-law hardens. The former spectrum was measured for RE J2248-511 in 1993 by the PSPC (although the slope of the hard X-ray power law was poorly constrained due to the limited range

of the PSPC) and the latter by *ASCA* in 1997. Even taking account of pessimistic systematic and cross-calibration errors, the changes between the two spectra are significant. An alternative model to the GBHC analogy is that the opacity in a hot, optically-thin corona surrounding an accretion disc has fallen.

The extreme patterns of variability observed in the X-ray and optical spectra of RE J2248-511 reveal a fascinating, highly dynamic source which can reveal much about the physics in the central regions and their relationship with the outer line-emitting gas. With the sparse, non-simultaneous data in hand, firm conclusions are difficult to draw. Optical and X-ray monitoring are essential to proceed further with investigations of this AGN.

ACKNOWLEDGMENTS

We thank Keith Mason for his advice. We also thank D. Grupe and H-C. Thomas for allowing us to print their optical spectrum, and for useful comments on the paper. We would also like to thank the referee for some constructive and useful comments leading to an improved paper.

REFERENCES

- Arnaud K.A. et al., 1985, *MNRAS*, 217, 105
 Baldwin J., Ferland G., Korista K., Verner D., 1995, *ApJ*, 455, L119
 Bevington P.R., 1969, *Data Reduction and Error Analysis for the Physical Sciences* (New York: McGraw-Hill)
 Boller Th., Brandt W.N., Fink H., 1996, *A&A*, 305, 53
 Brandt W.N., Fabian A.C., Nandra K., Reynolds C.S., Brinkmann W., 1994, *MNRAS*, 271, 958
 Brandt W.N., Pounds K.A., Fink H., 1995, *MNRAS*, 273, L47
 Brandt W.N., Mathur S., Elvis M., 1997, *MNRAS*, 285, L25
 Chakrabarti S.K., Titarchuk L.G., 1995, *ApJ*, 455, 623
 Collin-Souffrin S., Czerny B., Dumont A.M., Zycki P., 1996, *A&A*, 314, 393
 Comastri A., Setti G., Zamorani G., Elvis M., Wilkes B.J., McDowell J.C., Giommi P., 1992, *ApJ*, 384, 62
 Córdova F.A., Kartje J.F., Thompson R.J.Jr., Mason K.O., Puchnarewicz E.M., Harnden F.R.Jr., 1992, *ApJS*, 81, 661
 Dotani T. et al., 1996, *ASCA News*, Issue 4
 Ebisawa K., Titarchuk L., Chakrabarti S.K., 1996, *PASJ*, 48, 59
 Fiore F., Elvis M., McDowell J.C., Siemiginowska A., Wilkes B.J., 1994, *ApJ*, 431, 515
 Fruscione A., 1996, *ApJ*, 459, 509
 George I.M., Turner T.J., Netzer H., Nandra K., Mushotzky R.F., Yaqoob T., 1998, *ApJS*, 114, 73
 Grupe D., Beuermann K., Mannheim K., Thomas H-C, Fink H.H., DeMartino D., 1995, *A&A*, 300, L21
 Grupe D., Beuermann K., Thomas H-C., Mannheim K., Fink H.H., 1998, *A&A*, 300, 25, (G98)
 Guainazzi M. et al., 1998, *A&A*, 339, 327
 Haardt F., Maraschi L., 1993, *ApJ*, 413, 507
 Haardt F., Maraschi L., Ghisellini G., 1997, *ApJ*, 476, 620
 Iwasawa K., Brandt W.N., Fabian A.C., 1998, *MNRAS*, 293, 251
 Iwasawa K., Fabian A.C., Nandra K., 1999, *MNRAS*, 307, 611
 Laor A., Fiore F., Elvis M., Wilkes B.J., McDowell J.C., 1994, *ApJ*, 435, 611
 Laor A., Fiore F., Elvis M., Wilkes B.J., McDowell J.C., 1997, *ApJ*, 477, 93 (L97)
 Marshall H.L., Fruscione A., Carone T.E., 1995, *ApJ*, 439, 90
 Mason K.O. et al., 1995, *MNRAS*, 274, 1194 (M95)
 Nandra K., George I.M., Mushotsky R.F., Turner T.J., Yaqoob T., 1997, *ApJ*, 477, 602
 Piro L., Massaro E., Perola G.C., Molteni D., 1988, *ApJ*, 325, L25
 Pounds K.A. et al., 1993, *MNRAS*, 260, 77
 Pounds K.A., Done C., Osborne J.P., 1995, *MNRAS*, 277, L5
 Press W.H., Flannery B.P., Teukolsky S.A., Vetterling W.T., 1989, *Numerical Recipes: The Art of Scientific Computing* (Cambridge: Cambridge Univ. Press)
 Puchnarewicz E. M., Mason K. O., Córdova F. A., Kartje J., Branduardi-Raymont G., Mittaz J. P. D., Murdin P. G., Allington-Smith J., 1992, *MNRAS*, 256, 589
 Puchnarewicz E.M., Branduardi-Raymont G., Mason K.O., Sekiguchi K., 1995a, *MNRAS*, 276, 1281, (P95)
 Puchnarewicz E.M., Mason K., Siemiginowska A., Pounds K.A., 1995b, *MNRAS*, 276, 20
 Puchnarewicz E.M. et al., 1996, *MNRAS*, 281, 1243
 Puchnarewicz E.M. et al., 1997, *MNRAS*, 291, 177
 Puchnarewicz E. M., Mason K. O., Breeveld A. A., Siemiginowska A., 1998, *Proc Conference on Accretion Processes*, Maryland
 Rees M.J., Netzer A., Ferland G.J., 1989, *ApJ*, 347, 640
 Schartel N. et al., 1996, *MNRAS*, 283, 1015
 Schmidt M., Green R.F., 1983, *ApJ*, 269, 352
 Stark A.A., Gammie C.F., Wilson R.W., Bally J., Linke R.A., Heiles C., Hurwitz M., 1984, private distributed tape
 Stark A.A., Gammie C.F., Wilson R.W., Bally J., Linke R.A., Heiles C., Hurwitz M., 1992, *ApJS*, 79, 77
 Tanaka Y., Inoue H., Holt S.S., 1994, *PASJ*, 46, L37
 Turner T.J., Pounds K.A., 1989, *MNRAS*, 240, 833
 Walter R., Fink H.H., 1993, *A&A*, 274, 105
 Wang T., Otani C., Matsuoka M., Cappi M., Leighly K. M., Brinkmann W., 1998, *MNRAS*, 293, 397
 Wells A.A. et al., 1990, *SPIE*, 1344, 230

This paper has been produced using the Royal Astronomical Society/Blackwell Science \TeX macros.